Available online at www.sciencedirect.com
SCIENCE DIRECT
Electrochimica Acta 51 (2006) 2012–2022
ELECTROCHIMICA Acta
www.elsevier.com/locate/electacta

A generalized cycle life model of rechargeable Li-ion batteries

Gang Ning, Ralph E. White, Branko N. Popov *

Department of Chemical Engineering, University of South Carolina, Columbia, SC 29208, USA

Received 19 October 2004; received in revised form 26 April 2005; accepted 25 June 2005
Available online 15 August 2005

Abstract

A generalized first principles based charge–discharge model to simulate the cycle life behavior of rechargeable Li-ion batteries has been developed. The model is based on loss of the active lithium ions due to the electrochemical parasitic reaction and rise of the anode film resistance. The effect of parameters such as depth of discharge (DOD), end of charge voltage (EOCV) and overvoltage of the parasitic reaction on the cycle life behavior has been quantitatively analyzed. The experimental results obtained at charge rate of 1 C, discharge rate of 0.5 C, EOCV of 4.0 V and DOD of 0.4 were used to validate the cycle life model. Good agreement between the simulations and the experiments has been achieved up to 1968 cycles. Simulation of a battery subjected to multiple cycling regimes has also been demonstrated.
© 2005 Elsevier Ltd. All rights reserved.

Keywords: Cycle life; Capacity fade; Charge–discharge; First principles; Parasitic reaction

1. Introduction

Computer simulation provides the most efficient tool for reducing testing time and optimizing battery systems [1–3]. Darling and Newman [4] made a first attempt to model the parasitic reaction in Li-ion batteries by assuming a solvent oxidation reaction. Later, Spotnitz [5] developed polynomial expressions for the estimation of irreversible and reversible capacity loss due to the growth and dissolution of SEI film in Li-ion batteries. Ramadass et al. [6] developed a capacity fade prediction model for Li-ion cells based on a semi-empirical approach. Recently, Christensen and Newman [7] simulated the influence of anode film resistance on charge/discharge performance of a Li-ion battery. In their model, loss of cyclable lithium ions and increase in the anode film resistance were incorporated into the galvanostatic charge/discharge model previously developed by Doyle et al. [8].

We recently developed a first principles based charge–discharge model that neglects transport of lithium in electrolyte phase under low charge/discharge current [9–10]. As a result of the simplification, the computer modeling time has been efficiently shortened. With this model, the capacity fade of a battery is correlated with charge rate (CR), depth of discharge (DOD), end of charge voltage (EOCV) and discharge rate (DR). However, the model's limitation to only low charge/discharge rates (i.e. lower than 1 C) prevents its application to the conditions where charge/discharge rate may be 2 C, 3 C or even higher.

This paper describes a generalized charge–discharge model based on loss of the active lithium ions due to electrochemical solvent reduction reaction at anode/electrolyte interface. Simultaneous transport in both solid phase and electrolyte phase makes this model applicable not only for mild but also for harsh charge/discharge conditions. The rise in the anode film resistance is used to explain decrease of the discharge voltage plateau as a battery ages with cycling. The charge–discharge cycling process is first simulated to continuously update parameters such as the anode film resistance, R_f, and the lithium concentration in the anode at the beginning of discharge, c_s^0. Next, the program outputs those values to the subsequent simulation of capacity check to obtain the charge/discharge performance at a specific cycle number. All the simulations are carried out using Compaq Visual Fortran. The model has been validated against experimental data collected under a given condition, which has been utilized to expedite the degradation process to evaluate cycle life of a battery. It takes a PC with Pentium® 2.0 GHz CPU and

* Corresponding author. Tel.: +1 803 777 7314; fax: +1 803 777 8265.
E-mail address: popov@engr.sc.edu (B.N. Popov).

0013-4686/$ – see front matter © 2005 Elsevier Ltd. All rights reserved.
doi:10.1016/j.electacta.2005.06.033

512 Mb RAM 15 h to complete the simulation for ∼2000 charge–discharge cycles. This represents a significant advantage over experimental data collection, which took almost a year. Applying this model to cycle life behavior of a battery under multiple cycling regimes is also presented.

2. Experimental

The experiments were performed on rechargeable Li-ion batteries with a rated capacity of 1.67 Ah. The active electrode materials are Li_xCoO_2 cathode and MCMB anode. The electrolyte consists of 1 M $LiPF_6$ in a mixture of EC:PC:EMC:DEC (30:5:35:30). The cycling condition was controlled by the use of following parameters: end of charge voltage of 4.0 V, depth of discharge of 0.4, constant current–constant voltage (CC–CV) charge mode with cutoff current of 50 mA, charge rate of 1 C and discharge rate of 1/2 C.

The capacity was checked under the following conditions: EOCV of 4.2 V, end of discharge voltage (i.e. cutoff voltage) of 3.0 V, CC–CV charge protocol with cutoff current of 50 mA, discharge rate of 1/2 C and charge rate of 1/5 C.

3. Model development

Fig. 1 presents a one-dimensional schematic of a rechargeable Li-ion battery. During discharge, lithium ions deintercalate from MCMB negative electrode and intercalate into Li_xCoO_2 positive electrode. Inside porous electrode, intercalation/deintercalation processes take place at solid electrode/electrolyte interface. The model developed in this paper considers porous electrode theory, concentrated solution theory, Ohm's law, intercalation/deintercalation kinetics and transport in solid phase and electrolyte phase. To determine influence of a specific cycling protocol on the cycle life behavior of a rechargeable Li-ion battery, CV charge step, which has been neglected in most battery performance models is also taken into account in addition to CC charge process. The end of discharge process in the simulations of cycling process determines the starting point of next charge process. No rest time exists between charge and discharge processes or between cycling process and capacity check.

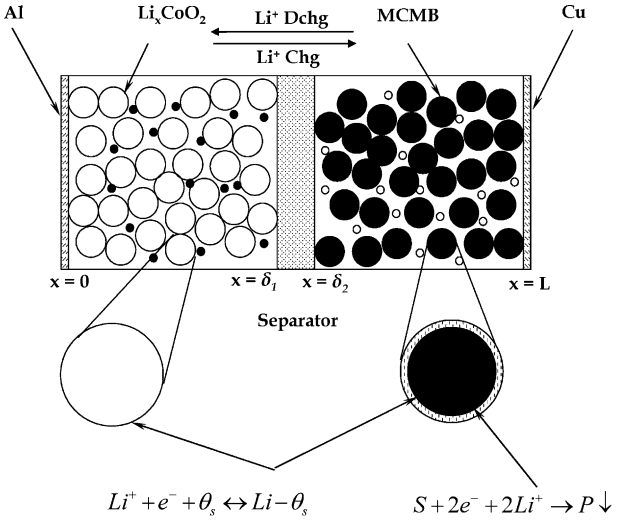

Fig. 1. Schematic of a rechargeable Li-ion battery.

It is been experimentally revealed the surface film formed during initial formation period over carbon electrode may not be able to fully accommodate volume change due to subsequent intercalation/deintercalation of lithium or due to accumulation of the gaseous by-products as a battery is subjected to cycling. A continuous small-scale reduction may take place on the anode when solvent percolates through the cracks on the surface film [11,14–18]. As a consequence, part of the cyclable lithium can be irreversibly lost to this parasitic reaction. It is assumed in our model the solvent, specifically the ethylene carbonate (EC), undergoes two-electron reduction at the anode/electrolyte interface during charge process, thus precipitating an insoluble film (a newly formed SEI layer) over the surface of the anode particles.

$$\mathrm{EC} + 2\mathrm{e}^- + 2\mathrm{Li}^+ \rightarrow \mathrm{LiCH_2CH_2OCO_2Li} \downarrow \quad (1)$$

No parasitic reaction was considered at Li_xCoO_2/electrolyte interface at any time. Other assumptions include: (i) only solid and liquid phases are involved, (ii) the electrolyte can be approximated by a concentrated binary electrolyte, (iii) intercalation/deintercalation reaction takes place only at the solid electrode/electrolyte interface and follows the Butler–Volmer equation, (iv) transport of ionic species in the electrolyte phase is by diffusion and migration, (v) transport of intercalated lithium in the solid phase is by diffusion, (vi) volume change is neglected during lithium intercalation/deintercalation, (vii) electrode porosity remains constant during cycling, (viii) electrochemical solvent reduction takes place only at anode/electrolyte interface and follows the Tafel equation, (ix) loss of cyclable lithium is irreversible, (x) mass transfer of cyclable lithium and reactive solvent (EC) through the anode SEI layer is unlimited, (xi) active electrode materials consist of spherical particles of a uniform size and (xii) heat generation and dissipation are negligible.

The governing equations and boundary conditions required in modeling the cycle life of rechargeable Li-ion batteries have been listed in Appendix A. Due to the irreversible nature of parasitic reaction, not all cyclable lithium intercalates back into anode material, which is responsible for the lithium concentration in the anode at the beginning of next discharge process being smaller at a given cycle than in the previous cycle. The volume-averaged loss can be estimated using the following equation:

$$Q_\mathrm{s} = \left| \int_{t=0}^{t=t_\mathrm{para}} j_\mathrm{para} a_\mathrm{s,n} \, \mathrm{d}t \right| \quad (2)$$

Table 1
Parameters used in the cycle life model of rechargeable Li-ion batteries

Parameter	Cathode (Li_xCoO_2)	Membrane separator (Celgard®)	Anode (MCMB)	References
Thickness (m)	7.4×10^{-5}	2.5×10^{-5}	7.5×10^{-5}	Manufacture
$c_{s,max}$ (mol/m^3)	51555		30555	[9]
c_e^0 (mol/m^3)	1000	1000	1000	[8,9]
D_s (m^2/s)	1.0×10^{-13}		3.8×10^{-14}	[8,9]
D_e (m^2/s)	2.5×10^{-10}	2.5×10^{-10}	2.5×10^{-10}	[8,9]
α_a/α_c	0.5		0.5	[8,9]
r_s (m)	2.0×10^{-6}		2.0×10^{-6}	[8,9]
k (A m$^{2.5}$/(C mol$^{0.5}$))	1.0×10^{-6}		1.0×10^{-6}	Assumed
σ_s (S/m)	10.0	0.0	100.0	[8,9]
κ_e (S/m)	2.5	2.5	2.5	[8,9]
ε_e	0.338	0.37	0.440	Manufacture
ε_{fl}	0.142		0.07	Assumed
t_+^0	0.2	0.2	0.2	[8,9]
S (m^2)	0.011		0.011	Manufacture

Accordingly, the lithium concentration in the anode at the beginning of discharge is modified at the end of charge by

$$c_s^0\big|_{N+1} = c_s^0\big|_N - \frac{Q_s}{F\varepsilon_s} \tag{3}$$

As a consequence of the continuous precipitation of the insoluble product ($LiCH_2CH_2OCO_2Li\downarrow$) over anode surface, the SEI film becomes thicker and thicker, thus leading to the rise in the anode film resistance.

$$R_f|_{N+1} = R_f|_N + R_f|_{para,N} \tag{4}$$

where the increased resistance due to accumulation of the insoluble product at anode surface at cycle number N, $R_f|_{para,N}$, is related to the increased film thickness, δ_f, at that specific cycle number by

$$R_s|_N = \frac{\delta_f|_N}{\kappa} \tag{5}$$

Volume balance of the precipitated insoluble product over the entire anode surface yields

$$\frac{\partial \delta_f|}{\partial t} = -\frac{j_{para}|\times M}{\rho \times F} \tag{6}$$

The cell parameters are listed in Tables 1 and 2. In the simulations, Eqs. (10), (12), (14), (19) and (20) as shown in Appendix A, need to be solved simultaneously for five dependent variables, i.e. C_e, ϕ_s, ϕ_e, C_s and $C_{s/e}$. The required open circuit potential of anode and cathode is shown in Appendix B. At the end of charge process, the lithium concentration in the anode, c_s^0, and the anode film resistance, R_f, should be updated using Eqs. (3) and (4). For the estimation of the charge/discharge performance at a specific cycle number, the simulation of cycling process needs to be run first in order to output values of c_s^0 and R_f to the subsequent simulation of capacity check.

Table 2
Values of parameters used for the parasitic reaction

Parameter	Value	References
U_{para} (V)	0.38	Assumed
M (kg/mol)	0.1	Based on Eq. (1)
ρ (g/m^3)	2.1×10^3	Based on Eq. (1)
j_{para}^0 (A/m^2)	0.80×10^{-7}	Assumed
κ_f (S/m)	3.79×10^{-7}	Assumed

4. Results and discussion

4.1. Simulation of charge–discharge performance

Figs. 2 and 3 present simulations of cell voltage and cell current density as a function of capacity, respectively. The simulations were carried out to mimic the initial CC–CV charge and CC discharge cycle. The cell voltage shown in Fig. 2 is defined to be the difference in the potential of the solid phase (ϕ_s) at the positive end ($x = 0$) and at the negative end ($x = L$) of a Li-ion battery. Based on the rated capacity and the geometric surface area of the electrode, charge/discharge rate of 1 C corresponds to current density of 19.0 A/m^2. Despite noticeable differences in the charge characteristics (including voltage and current) at different charge rates, as shown

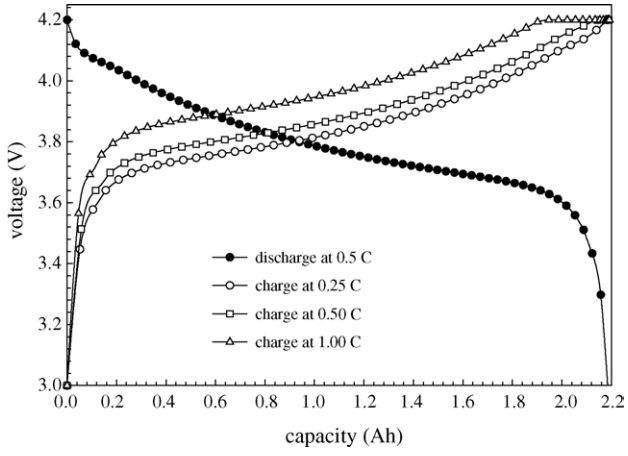

Fig. 2. Simulations of initial charge–discharge voltage profiles.

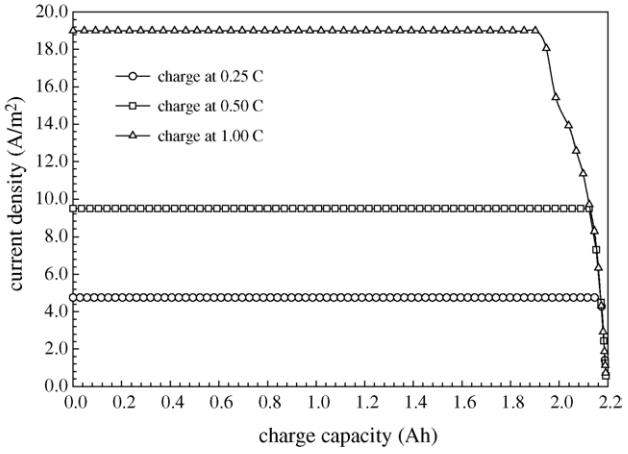

Fig. 3. Simulations of initial charge current profiles.

in Figs. 2 and 3, the initial discharge performance including (voltage plateau and capacity) remains identical at the same discharge rate of 1/2 C. These results have shown the importance of CV charge step and the setting cutoff current to be 50 mA. Fig. 3 also shows a decrease in the CC charge capacity as charge rate increases. The percentage of capacity gained during CV charge step increases with increase in the charge rate as a result of the resistive characteristics of a battery. For charge rate of 1 C, roughly 10% of the capacity has been estimated to be supplied by the CV charge mode.

The initial state of charge (SOC) of anode or cathode at fully charged state is difficult to determine precisely due to different manufacturing processes and the loss of cyclable lithium in the initial formation period. The estimated values from fitting initial experimental discharge curves are

$$\frac{c^0_{s,p}}{c^0_{s,p,max}} = 0.48 \quad \text{and} \quad \frac{c^0_{s,n}}{c^0_{s,n,max}} = 0.83 \tag{7}$$

Fig. 4 shows how concentration profile of $LiPF_6$ in the electrolyte phase varies with time along the current flow direction in the first discharge–charge cycle. The charge rate is 1 C and the discharge rate is 0.5 C. As CC charge process starts, the salt $LiPF_6$ moves from the anode toward the cathode, thus yielding a negative concentration gradient inside cathode, membrane separator and anode. As CC charge proceeds, the concentration gradient increases gradually along the current flow path and reaches the maximum at the beginning of CV charge (i.e. the end of CC charge). During CV charge, the applied current drops rapidly, thus causing the $LiPF_6$ concentration gradient to decrease from the maximum to a trivial level as CV charge reaches the end. Consequently, system returns to a quasi-steady-state after cyclable lithium has intercalated back into anode. This phenomenon has justified our estimation for the volume-averaged loss, Q_s, by the use of Eq. (3). The $LiPF_6$ concentration profile during discharge presents a positive gradient, which increases as discharge proceeds until discharge process reaches the end. It is also shown in Fig. 4 that the maximum concentration gradient (absolute value of the difference of $LiPF_6$ from anode to cathode) depends upon the charge/discharge rate applied. For charge rate of 1 C, the concentration varies from 1155 mol/m^3 to 885 mol/m^3 (cathode to anode), while for discharge rate of 1/2 C, it varies from 920 mol/m^3 to 1060 mol/m^3 (cathode to anode) representing the largest concentration gradient during charge and discharge process, respectively.

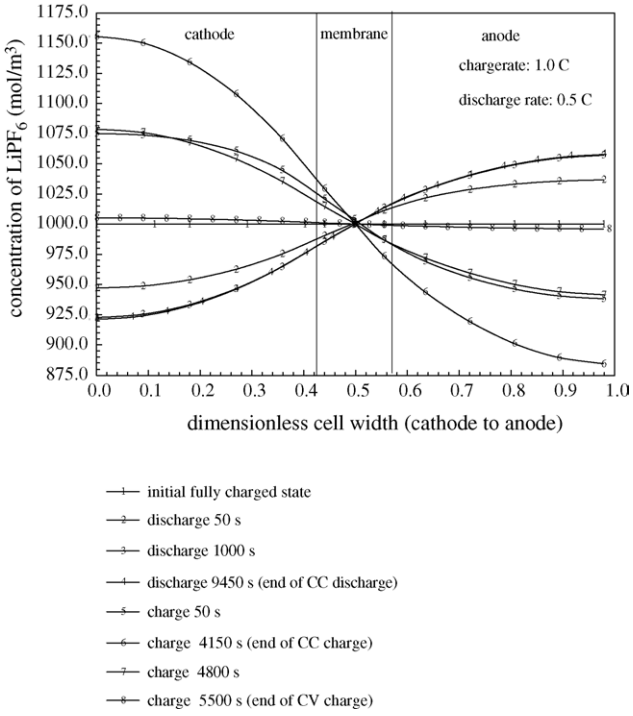

Fig. 4. Simulations of lithium concentration in the electrolyte phase.

4.2. Simulation of cycling performance

Fig. 5 shows simulations of the first four charge–discharge cycles. The simulations were performed for EOCV of 4.0 V, DOD of 0.4, CR of 1.0 C and DR of 0.5 C. Since CR of 1.0 C was used, CV is primarily responsible for the capacity as shown in Fig. 5. It is been estimated that 70% of the capacity is supplied by CV charge in the first charge process. As a battery ages, a gradual decrease of the end of discharge cell voltage corresponding to a specific DOD is observed (corresponding to point "a" in Fig. 5). Since no parasitic reaction was assumed at cathode, the potential of cathode at the aluminum foil/Li_xCoO_2 interface (i.e. $x = 0$) always cycles within such a range as it is required by DOD of 0.4 and EOCV of 4.0 V, i.e. back and forth between point "A" and "B" in Fig. 6. Because capacity fade occurs in cycling process, part of the cyclable lithium becomes irreversibly lost due to the electrochemical parasitic reaction, thus resulting, according to Eqs. (2) and (3), in a gradual decrease of the initial lithium concentration in the anode at the beginning of discharge. As shown in Fig. 6, SOC of anode at the beginning of discharge potential has moved from "C" to "C′" after 1000 cycles. To maintain

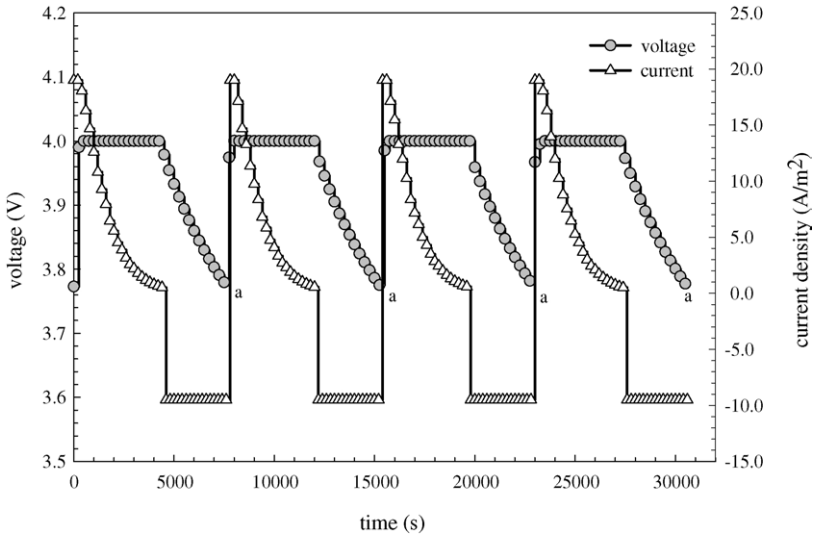

Fig. 5. Simulations of charge–discharge cycling process (CR: 1 C; DR: 0.5 C; EOCV: 4.0 V; DOD: 0.4).

the required DOD, the SOC of anode at the end of discharge has to be shifted from "D" to "D′" accordingly. The end of discharge cell voltage is the difference in the solid phase potential of cathode at $x = 0$ and the solid phase potential of anode at $x = L$,

$$V|_{N=1} = \phi_s|_B - \phi_s|_D \quad \text{and} \quad V|_{N=1000} = \phi_s|_B - \phi_s|_{D'} \tag{8}$$

Since, according to Eq. (36), $\phi_s|_{D'}$ is greater than $\phi_s|_D$, the end of discharge cell voltage decreases as cycle number increases. When high values of EOCV and DOD are used to charge–discharge a battery, $\phi_s|_{D'}$ can be forced to move toward SOC of 0% at a fast rate as a consequence of fast capacity fade. Hence at a certain point during cycling, the output voltage can be lower than the cutoff of 3.0 V in order to maintain the specified DOD, which marks the end of the cycle life.

4.3. The parasitic reaction at anode/electrolyte interface

As defined by Eq. (16) in Appendix A, the electrochemical parasitic reaction current density depends upon the overpotential. As the potential of anode and cathode varies, the overpotential also varies. Fig. 7 shows the overpotential as a function of charge time in the first charge cycle (i.e. from DOD of 0.4 to EOCV of 4.0 V using CC–CV charge). Since the open circuit potential of the parasitic reaction

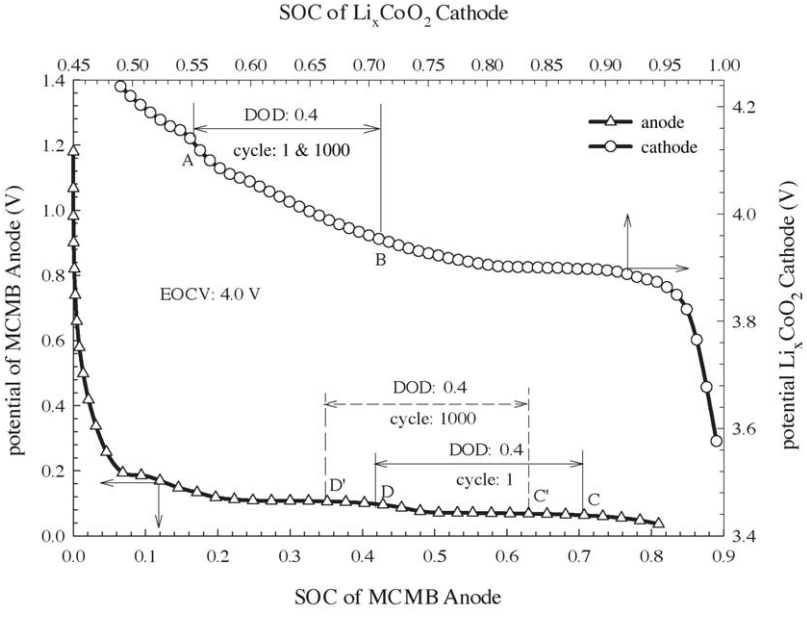

Fig. 6. Potential of individual electrode vs. SOC.

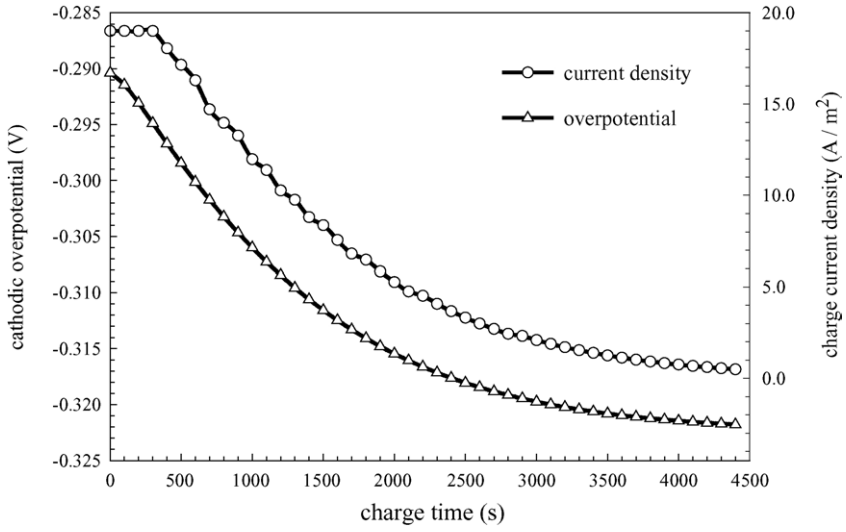

Fig. 7. Overpotential vs. charge time in the first charge cycle.

was assumed to be 0.38 V, which essentially determines the characteristics of cathodic overpotential in the Tafel equation, the parasitic reaction takes places immediately at the beginning of charge. The absolute value of the overpotential increases faster during most of the CC–CV charge time and more slowly toward the end of CV charge. The loss of cyclable lithium is calculated with Eq. (2). It is estimated that 5.5% of the cyclable lithium loss occurred during the CC charge mode, while 94.5% took place in the CV charge mode. Thus, models that do not consider the CV charge mode can inevitably introduce large errors in predicting the cycle life of a battery.

The dependence of lithium concentration in the solid phase as a function of charge process is schematically shown in Fig. 8. During the CC charge mode, the reversible lithium is transported from the cathode/electrolyte interface to the anode/electrolyte interface. As shown in Fig. 8A, as a result of the fast intercalation/deintercalation as well as the fast transport in the electrolyte phase, the lithium concentration at the cathode/electrolyte interface is lower than the bulk lithium concentration in the cathode. Similarly, the lithium concentration at the anode/electrolyte interface is higher than the bulk lithium concentration in the anode. Since the local equilibrium potential is a function of the lithium concentration at the solid/electrolyte interface, $C_{s/e}$, the end of charge voltage (i.e. 4.0 V) can be reached after a certain duration with CC charge. Before that point, the potential of the anode particle decreases rapidly according to Eq. (36) in Appendix B. However, the potential of the electrolyte phase does not decrease as much as the potential in the solid phase. Hence, the absolute value of the overpotential of the parasitic reaction increases according to Eq. (16) as shown in Fig. 7. After the CC charge is over, the accumulated lithium at the anode/electrolyte interface diffuses into the bulk of the anode. The lithium in the bulk of the cathode diffuses to the cathode/electrolyte interface and becomes free lithium ion through deintercalation. As shown in Fig. 8B, the lithium concentration becomes almost homogeneous in the anode as well as in the cathode at the end of the CV charge. The potential of the anode particles increases because of a decrease in $C_{s/e,n}$. The potential of the

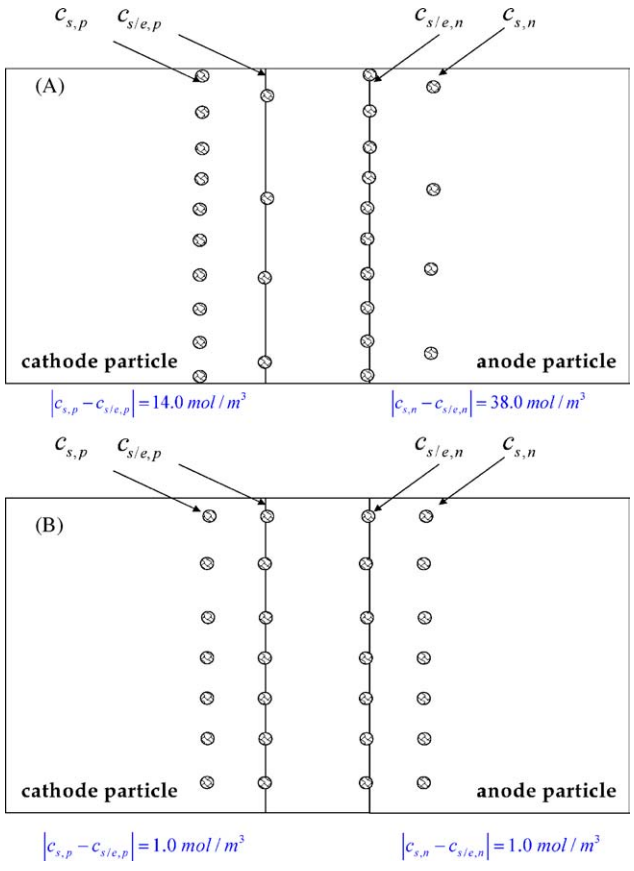

Fig. 8. Variation of lithium concentration in the solid phase during CC–CV charge at $x = 0$ and $x = L$ at the end of: (A) constant current charge and (B) constant voltage charge.

cathode increases as a result of the increase in $C_{s/e,p}$. The difference of these two potentials is controlled by the external circuit. The detailed discussion concerning the change in the driving force (i.e. the concentration gradient within the solid particles) was discussed in our previous work [10].

Only a small variation in the potential of the electrolyte phase is observed in the CV charge mode. The current density across the solid/electrolyte interface, j, in Eq. (16) has a negative value for charge process. Thus, whether the absolute value of the overpotential increases or decreases mainly depends on the potential of the anode, ϕ_s, and the ohmic drop across the anode surface film, jR_f. In our simulations, the observed fast decay of the charge current from 1.67 A (1 C) to the cutoff current of 50 mA contributes more to the continuous increase of absolute value of the overpotential as shown in Fig. 7. But as the current decreases, the increase rate also decreases.

The influence of EOCV and DOD has been analyzed in our previous study [10]. These two factors affect the rate of the loss of the cyclable lithium according to Eqs. (2) and (16). Higher values of EOCV or DOD always contribute to a faster capacity fade.

4.4. Comparison of simulated and experimental discharge curves at different cycles

To test the validity of the model and the proposed mechanism of the capacity fade, the discharge voltage curves at 1, 822, 1124 and 1968 cycles were simulated based on the parameters listed in Tables 1 and 2. Some of the parameters in the tables were not be able to precisely measure. So they were either assumed or obtained by fitting the model against the discharge curves in the early period of cycle life of our batteries. Fig. 9 presents a comparison of the model predictions and the experimental results. Good agreement is observed for the voltage plateau and for the capacity. The relative error in the discharge capacity is less than 2.0% after

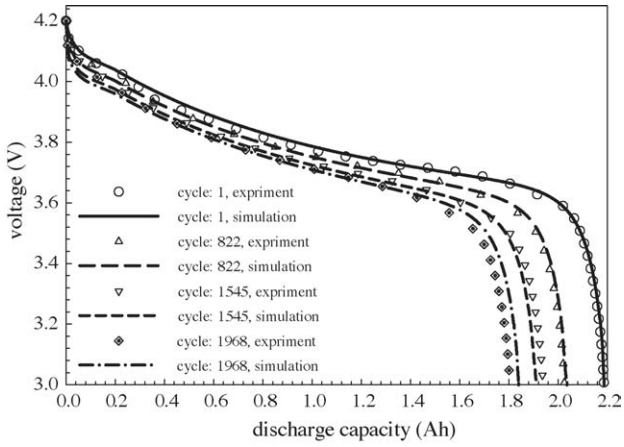

Fig. 9. Comparisons of model predictions and experimental results.

1968 cycles. Fig. 10 presents the estimated lithium concentration of the anode at the beginning of discharge and anode film resistance versus cycle number. The concentration decreases from cycle to cycle according to Eq. (3) and the film resistance increases according to Eq. (4). This model predicts an increase in the anode film resistance from $8.7 \times 10^{-3}\,\Omega\,m^2$ initially to $15.1 \times 10^{-3}\,\Omega\,m^2$ after 1968 cycles.

4.5. Simulations of cycle life with multiple cycling regimes

In real life applications, a battery might be operated under multiple cycling regimes according to power and voltage requirements. As a consequence, the control parameters used in the system, i.e. EOCV, DOD, CR and DR, may be used in different combinations. Simulating the cycle life and the capacity fade of a battery subjected to multiple cycling regimes requires the model be able to incorporate those four parameters. Fig. 11 presents the discharge–charge cycles under six consecutive cycling protocols characterized by—(I)

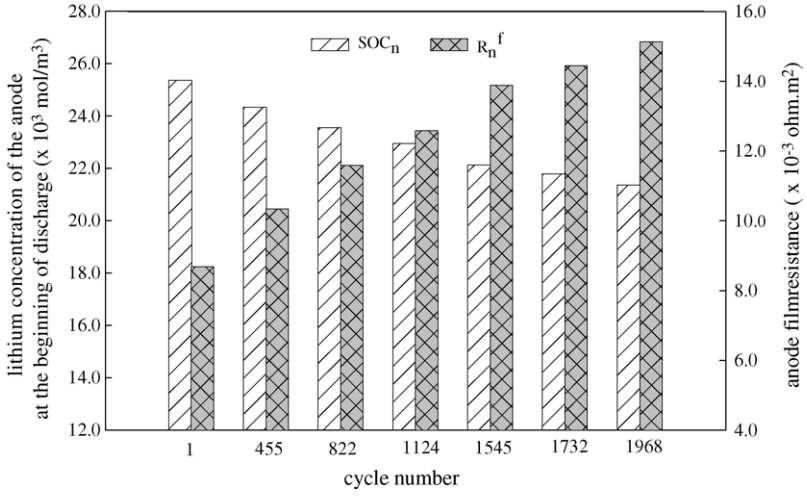

Fig. 10. The lithium concentration of the anode at the beginning of discharge and the anode film resistance vs. cycle number.

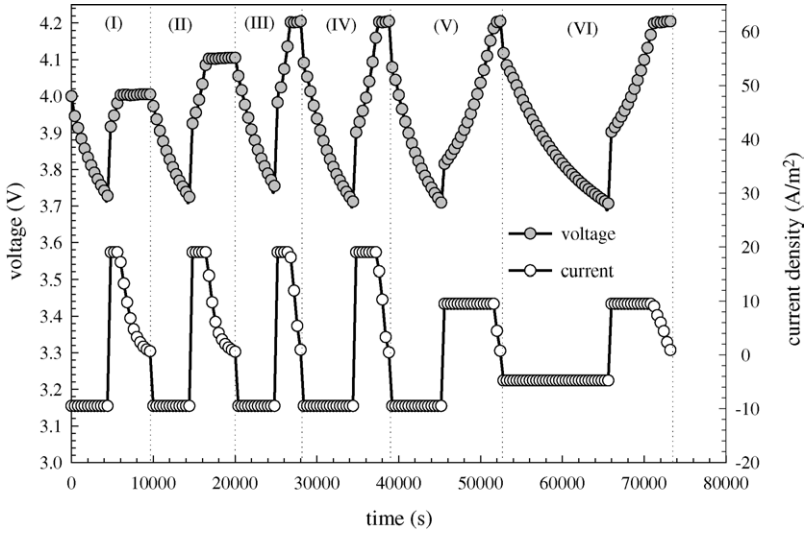

Fig. 11. Simulations of the cycling process of the battery under multiple cycling regimes.

EOCV: 4.0 V, DOD: 0.5, CR: 1 C, DR: 0.5 C; (II) EOCV: 4.1 V, DOD: 0.5, CR: 1 C, DR: 0.5 C; (III) EOCV: 4.2 V, DOD: 0.5, CR: 1 C, DR: 0.5 C; (IV) EOCV: 4.2 V, DOD: 0.7, CR: 1 C, DR: 0.5 C; (V) EOCV: 4.2 V, DOD: 0.7, CR: 0.5 C, DR: 0.5 C; (VI) EOCV: 4.2 V, DOD: 0.7, CR: 0.5 C, DR: 0.25 C.

To show the difference in the simulated voltage/current profiles between adjacent cycles, only one parameter was varied. The lithium concentration of the anode at the beginning of discharge, c_s^0, and the film resistance at the anode, R_f, need to be updated at the end of each discharge–charge cycle as discussed above. After a certain cycle number, simulation of the capacity fade can be initiated to estimate the charge/discharge performance and the capacity.

5. Conclusion

A generalized charge–discharge cycle life model has been developed based on loss of cyclable lithium ions due to the irreversible solvent reduction reaction. The rise in the anode film resistance due to the precipitation of insoluble product of the parasitic reaction has been used to explain the shift of the voltage plateau as a battery ages with cycling. The model considers process parameters such as CR, DOD and EOCV, controls the required DOD by controlling the discharge time, and estimates the end of discharge cell voltage corresponding to a specific DOD shifts downwards as a battery ages. The cycling process has been simulated to update the variables, c_s^0 and R_f, and the capacity check has been simulated to estimate the charge/discharge behavior as well as the capacity using those two updated variables. Experimental results obtained at a cycling condition with CR of 1 C, EOCV of 4.0 V, DOD of 0.4 and DR of 0.5 C have been used to validate the cycle life model. Good agreement between simulations and experiments up to 1968 cycles has been observed. Simulation of batteries under multiple cycling regimes has also been demonstrated.

Appendix A

The derivations of the following governing/boundary equations have been discussed in literature [8,19].

A.1. Model equations

For the spherical particles of electrode materials under ideally close packing condition, the specific interfacial area of the porous electrode is calculated by

$$a_s = \frac{3\varepsilon_s}{r} = \frac{3 \times (1 - \varepsilon_e - \varepsilon_{fl})}{r} \tag{9}$$

where ε_s, ε_e and ε_{fl} represent the volume fraction of solid active material, electrolyte and current conductive fillers, respectively, in the electrode regions.

For the mass balance in the electrolyte phase,

$$\frac{\partial(\varepsilon_e c_e)}{\partial t} = \nabla \cdot (D_e^{eff} \nabla c_e) - \frac{i_e \nabla t_+^0}{F} + \frac{1 - t_+^0}{F} a_s j \tag{10}$$

where the transference number, t_+^0, in reference to the velocity of solvent is assumed to be constant due to the lack of data in literature. The effective diffusion coefficient inside the porous electrode, D_e^{eff}, is evaluated by the Bruggeman relation [8],

$$D_e^{eff} = D_e \varepsilon_e{}^{1.5} \tag{11}$$

For Ohm's law in the solid phase

$$\nabla \cdot (\sigma_s^{eff} \nabla \phi_s) - a_s j = 0 \tag{12}$$

where the effective conductivity of the solid phase, σ_s^{eff}, is related to the intrinsic conductivity of the active materials,

σ_s, through the volume fraction of the solid active material, ε_s as follows:

$$\sigma_s^{eff} = \sigma_s \varepsilon_s{}^{1.5} \tag{13}$$

For Ohm's law in the electrolyte phase

$$\nabla \cdot (\kappa_e^{eff} \nabla \phi_s) + \nabla \cdot \left(\frac{2RT\kappa_e^{eff}}{F} (t_+^0 - 1) \left(1 + \frac{d \ln(f_\pm)}{d \ln c_e} \right) \nabla \phi_s \right) + a_s j = 0 \tag{14}$$

where the effective ionic conductivity is corrected by $\kappa_e^{eff} = \kappa_e \varepsilon_e^{1.5}$, following the Bruggeman relation [8]. The mean molar activity coefficient of salt, $f_\pm$, is assumed to be constant under normal operating temperature and pressure.When the parasitic reaction takes place at the anode/electrolyte interface, the wall flux across the interface, j, is given by

$$j = j_{int} + j_{para} \tag{15}$$

where the local parasitic reaction current density, j_{para}, is assumed to follow a simple Tafel relation.

$$j_{para} = -j_{para}^0 \exp\left(\frac{\alpha_c F}{RT} \eta \right)$$
$$\eta = \phi_s - \phi_e - U_{para} - jR_f \tag{16}$$

In the absence of parasitic reaction, the wall flux across anode/electrolyte interface or cathode/electrolyte interface is equal to the local intercalation/deintercalation current density.

$$j = j_{int} \tag{17}$$

where the intercalation/deintercalation current density, j_{int}, is given by the Butler–Volmer equation.

$$j_{int} = Fk(c_e)^{\alpha_a} (c_{s,max})^{\alpha_a} (c_{s/e})^{\alpha_a} \times \left(\exp\left(\frac{\alpha_a F}{RT} \eta \right) - \exp\left(\frac{\alpha_c F}{RT} \eta \right) \right)$$
$$\eta = \phi_s - \phi_e - U_{ref} - jR_f$$
$$R_f = 0, \quad \text{for cathode}$$
$$R_f|_{N+1} = R_f|_N + R_f|_{para,N}, \quad \text{for anode} \tag{18}$$

where $c_{s/e}$ represents the lithium concentration of the solid phase at the solid electrode/electrolyte interface and $c_{s,max}$ is the maximum concentration in the solid phase (corresponding to unit stoichiometry).

The rigorous model equation to describe the transport in the solid spherical particles is Fick's second law. After the free lithium becomes intercalated lithium on the surface of the particles, the intercalated lithium starts diffusing into the bulk of the solid electrode particles. However, the consideration for the transport in the radial direction increases the difficulties in modeling the battery system because the diffusion equation is coupled with all the other equations by the continuous flux condition at the solid particle/electrolyte interface. To simplify the pseudo-two-dimensional system, Doyle et al. [8] referenced Duhammel superposition method to calculate the mass flux across the solid electrode/electrolyte interface from all the previous surface concentration at each time points. The approximation proves to be efficient in their galvanostatic charge/discharge model. However, the cycle number in the cycle life model could be as high as thousands of cycles, so using all the previous concentration to calculate the flux at the interface is not as efficient as suggested in Dolye et al.'s paper [8].

The integral method [12] shows that a polynomial approximation leads to a satisfactory accuracy in solving the heat conduction problem. The second-degree polynomial representation was adopted in a thermal–electrochemical coupled model by Gu and Wang [13]. The diffusion equation and boundary conditions are thus replaced by a first-order differential equation and an algebraic equation that deal with the volume-averaged solid phase concentration (c_s) in addition to the lithium concentration of the solid phase at the electrode/electrolyte interface ($c_{s/e}$).

$$\frac{\partial(\varepsilon_s c_s)}{\partial t} = \frac{-a_s j_{int}}{F} \tag{19}$$

and

$$\frac{D_s}{l}(c_{s/e} - c_s) = \frac{-j_{int}}{F} \tag{20}$$

where the microscopic diffusion length that characterizes the lithium diffusion in the spherical particle, l, is given by [13]

$$l = \frac{r_s}{5} \tag{21}$$

As a result of this simplification, one more dependent variable, c_s, is introduced into the previous equations but the dimension of the system has been decreased to only x direction (cathode to anode).

A.2. Initial and boundary conditions

Initial conditions are:

$$c_e = c_e^0, \qquad c_s = c_{s/e} = c_s^0 \tag{22}$$

The boundary conditions for the concentration of the electrolyte phase (c_s) are:

$$\left. \frac{\partial c_e}{\partial x} \right|_{x=0} = 0 \tag{23}$$

$$\left. D_{e,p}^{eff} \frac{\partial c_e}{\partial x} \right|_{x=\delta_1^-} = \left. D_{e,m}^{eff} \frac{\partial c_e}{\partial x} \right|_{x=\delta_1^+} \tag{24}$$

$$\left. D_{e,m}^{eff} \frac{\partial c_e}{\partial x} \right|_{x=\delta_2^-} = \left. D_{e,n}^{eff} \frac{\partial c_e}{\partial x} \right|_{x=\delta_2^+} \tag{25}$$

$$\left. \frac{\partial c_e}{\partial x} \right|_{x=L} = 0 \tag{26}$$

The boundary conditions for the potential of the solid phase (ϕ_s) are:

$$-\sigma_{s,p}^{eff}\left.\frac{\partial\phi_s}{\partial x}\right|_{x=0} = i(t) = \frac{I_{app}}{S_p} \quad \text{(CC charge/discharge), or}$$
$$\phi_s|_{x=0} - \phi_s|_{x=L} = \text{EOCV} \quad \text{(CV charge)} \tag{27}$$

$$-\sigma_{s,p}^{eff}\left.\frac{\partial\phi_s}{\partial x}\right|_{x=\delta_1^-} = 0 \tag{28}$$

$$-\sigma_{s,n}^{eff}\left.\frac{\partial\phi_s}{\partial x}\right|_{x=\delta_2^+} = 0 \tag{29}$$

$$-\sigma_{s,n}^{eff}\left.\frac{\partial\phi_s}{\partial x}\right|_{x=L} = i(t) = \frac{I_{app}}{S_n} \quad \text{(CC charge/discharge), or}$$
$$\phi_s|_{x=0} - \phi_s|_{x=L} = \text{EOCV} \quad \text{(CV charge)} \tag{30}$$

The boundary conditions for the potential of the electrolyte phase (ϕ_e) are:

$$-\kappa_{e,p}^{eff}\left.\frac{\partial\phi_e}{\partial x}\right|_{x=0} = 0 \tag{31}$$

$$-\kappa_{e,p}^{eff}\left.\frac{\partial\phi_e}{\partial x}\right|_{x=\delta_1^-} = -\kappa_{e,m}^{eff}\left.\frac{\partial\phi_e}{\partial x}\right|_{x=\delta_1^+} \tag{32}$$

$$-\kappa_{e,m}^{eff}\left.\frac{\partial\phi_e}{\partial x}\right|_{x=\delta_2^-} = -\kappa_{e,n}^{eff}\left.\frac{\partial\phi_e}{\partial x}\right|_{x=\delta_2^+} \tag{33}$$

$$\phi_e = 0 \text{ (arbitrary reference)} \tag{34}$$

In summary, a total of five governing equations, i.e. Eqs. (10), (12), (14), (19) and (20), need to be solved simultaneously for the five dependent variables, i.e. c_e, ϕ_s, ϕ_e, c_s and $c_{s/e}$, with two independent variables, i.e. x and t.

Appendix B

The open circuit potential U_{ref} is a function of the lithium concentration of the solid phase at the solid electrode/electrolyte interface, $c_{s/e}$. The U_{ref} was estimated by fitting the experimental low-rate (1/20 C rate) charge/discharge voltage profile of the cathode and the anode as shown in Figs. 12 and 13. The experimental charge–discharge curves were obtained by charging and discharging the cathode and anode materials in a T-cell configuration [11].

For the cathode,

$$\begin{aligned} U_{ref,p} = {} & 14192290.6270 - 287201430.3900\theta_p^1 \\ & + 127581.0230\theta_p^2 - 15457341740.1321\theta_p^3 \\ & + 60863615826.7625\theta_p^4 - 173709561585.7754\theta_p^5 \\ & + 370555615410.3253\theta_p^6 - 600127143006.2673\theta_p^7 \\ & + 741424912055.3440\theta_p^8 - 695296927727.6394\theta_p^9 \\ & + 487165768837.1404\theta_p^{10} - 247280303663.7798\theta_p^{11} \\ & + 85951760175.1607\theta_p^{12} - 18311389879.7240\theta_p^{13} \\ & + 1803876860.8238\theta_p^{14} \end{aligned} \tag{35}$$

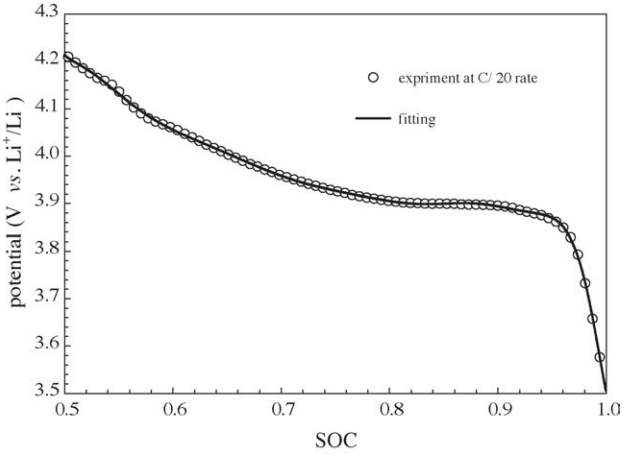

Fig. 12. Fitting open circuit potential (OCP) of Li_xCoO_2 T-cell.

For the anode,

$$U_{ref,n} = \frac{1.19970 + 118.1911\theta_n^{0.5} - 706.0711\theta_n + 2217.6479\theta_n^{1.5} - 1675.1321\theta_n^{2.0}}{1.0 + 131.7572\theta_n^{0.5} - 32.1402\theta_n - 746.8463\theta_n^{1.5} + 15502.9505\theta_n^{2.0} - 14213.0747\theta_n^{2.5}} \tag{36}$$

where the state of charge, θ_p/θ_n, is defined as

$$\theta_p = \frac{c_{s/e,p}}{c_{s,p,max}} \quad \text{and} \quad \theta_n = \frac{c_{s/e,n}}{c_{s,n,max}} \tag{37}$$

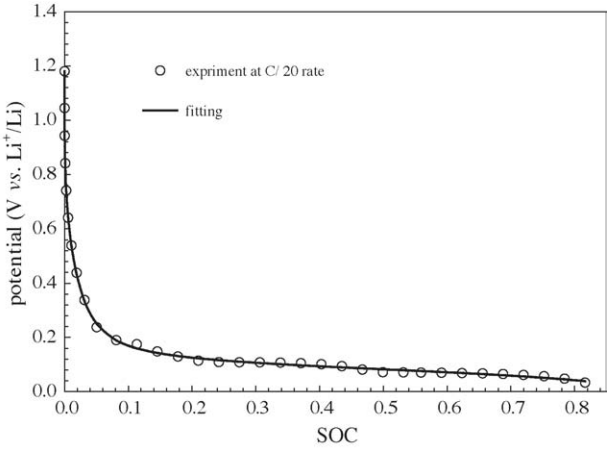

Fig. 13. Fitting open circuit potential (OCP) of MCMB T-cell.

Appendix C. Nomenclature

a	specific interfacial area of porous electrode (m^2/m^3)
c_s	lithium concentration of solid phase (mol/m^3)
$c_{s/e}$	lithium concentration of solid phase at electrode/electrolyte interface (mol/m^3)
D	diffusion coefficient (m^2/s)
F	Faraday's constant (96,487 C/mol)
i	current density (A/m^2)
I	current (A)
j	current density across electrode/electrolyte interface (A/m^2)
k	rate constant of lithium intercalation/deintercalation ($A\,m^{2.5}/(C\,mol^{0.5})$)
M	molecular weight (kg/mol)
Q	volume-averaged capacity lost due to parasitic reaction (C/m^3)
r	radius of particles (m)
R	universal gas constant (8.314 J/(mol K))
R_f	film resistance at the anode ($\Omega\,m^2$)
S	geometric surface area of electrode (m^2)
SOC	state of charge
t	time (s)
T	temperature (K)
U	local equilibrium potential (V)
V	battery output voltage (V)
X	thickness (m)

Greek letters

α^a/α^c	anodic/cathodic transfer coefficient of an electrochemical reaction
δ	thickness (m)
ε	volume fraction of a phase
ϕ	potential of a phase (V)
η	overpotential of an electrochemical reaction (V)
κ	conductivity of the newly formed surface film (S/m)
θ	active sites on the surface of electrode
ρ	density of film (kg/m^3)

Subscripts and superscripts

e	electrolyte phase
eff	effective
f	film
fl	current conductive filler
i	positive or negative electrode
int	intercalation/deintercalation
m	membrane separator
max	maximum value
N	cycle number
n	negative electrode
p	positive electrode
para	parasitic reaction
ref	in reference to Li^+/Li electrode
s	solid phase
s/e	solid/electrolyte interface
0	initial state

References

[1] T. Inoue, T. Sasake, N. Immamura, H. Yoshida, M. Mizutani, NASA Aerospace Battery Workshop, Huntsville, Alabama, 2001.
[2] I. Bloom, B.W. Cole, J.J. Sohn, S.A. Jones, E.G. Polzin, V.S. Battaglia, G.L. Henriksen, C. Motloch, R. Richardson, T. Unkelhaeuser, D. Ingersoll, H.L. Case, J. Power Sources 101 (2001) 238.
[3] M. Broussely, S. Hereyre, P. Biensan, P. Kasztejna, K. Nechev, R.J. Staniewicz, J. Power Sources 97–99 (2001) 13.
[4] R. Darling, J. Newman, J. Electrochem. Soc. 145 (1998) 990.
[5] R. Spotnitz, J. Power Sources 113 (2002) 72.
[6] P. Ramadass, B. Haran, R.E. White, B.N. Popov, J. Power Sources 123 (2003) 230.
[7] J. Christensen, J. Newman, J. Electrochem. Soc. 150 (2003) 1416.
[8] M. Doyle, T.F. Fuller, J. Newman, J. Electrochem. Soc. 140 (1993) 1526.
[9] G.P. Ramadass, B. Haran, P.M. Gomadam, R.E. White, B.N. Popov, J. Electrochem. Soc. 151 (2004) 196.
[10] G. Ning, B.N. Popov, J. Electrochem. Soc. 151 (2004) A1584.
[11] G. Ning, B.N. Popov, J. Power Sources 117 (2003) 160.
[12] M.N. Ozisik, Heat Conduction, John Wiley and Sons, 1993 (Chapter 9).
[13] W.B. Gu, C.Y. Wang, ECS Proceedings, vol. 99–25 (1), 2000, p. 748.
[14] D. Aurbach, E. Zinigrad, Y. Cohen, H. Teller, Solid State Ionics 148 (2002) 405.
[15] D. Aurbach, A. Zaban, Y. Ein-Eli, I. Weissman, O. Chusid, B. Markovsky, M. Levi, E. Levi, A. Schechter, E. Granot, J. Power Sources 68 (1997) 91.
[16] D. Aurbach, J. Power Sources 89 (2000) 206.
[17] Y.-G. Ryu, S.-I. Pyun, J. Electroanal. Chem. 97 (1997) 433.
[18] P. Ramadass, B. Haran, R.E. White, B.N. Popov, J. Power Sources 111 (2002) 210.
[19] J. Newman, Electrochemical System, second ed., Prentice Hall, New Jersey, 1991 (Chapter 22).